CERN - European Laboratory for Particle Physics

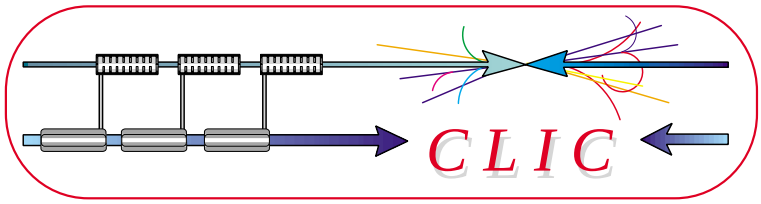

CLIC Note 470

Beam dynamics for the CTF3 preliminary phase

R. Corsini, A. Ferrari, L. Rinolfi, T. Risselada, P. Royer, F. Tecker

Abstract

In the framework of the CLIC RF power source studies, the new scheme of electron pulse compression and bunch frequency multiplication, using injection by RF deflectors into an isochronous ring, will be tested at CERN during the CTF3 preliminary phase. The present LPI complex will be modified in order to allow a test of this scheme at low charge. The design of the new front-end, of the modified linac, of the matched transfer line, and of the isochronous ring lattice is presented here. The results of the related beam dynamics studies are also discussed.

Geneva, Switzerland
January 30, 2001

Contents

1 Introduction

The Compact Linear Collider (CLIC)[1] RF power source is based on a new scheme of electron pulse compression and bunch frequency multiplication in which the drive beam time structure is obtained by the combination of electron bunch trains in isochronous rings using RF deflectors [1]. The next CLIC Test Facility (CTF3) will be built at CERN in order to demonstrate such a scheme and to provide a 30 GHz RF source with the CLIC nominal peak power and pulse length [2].

CTF3 will be installed in the area of the present LEP Pre-Injector (LPI) complex. Its construction is planned to proceed in stages over five years, as the new equipment will become available. In particular, the new linac, adapted to high charge operation with full beam-loading, should be ready for installation at the beginning of year 2003. Before this date, as a preliminary stage, a test of the bunch combination scheme at low charge is planned. This CTF3 preliminary stage will mainly make use of existing LPI components. A pulse train of up to five pulses will be accelerated in a linac and injected into a ring. Each pulse will be composed of several electron bunches, spaced by 10 cm (corresponding to the 3 GHz acceleration frequency). The distance between the pulses corresponds to the ring circumference, therefore the pulses can be combined turn after turn at the injection, by interleaving their bunches using RF deflectors. A single pulse with up to five times the initial pulse charge and up to five times the bunch repetition frequency will thus be obtained after combination.

The aim of this note is to present the beam dynamics studies for the CTF3 preliminary phase and to describe the necessary modifications of the existing installation.

[1] All acronymes are given in the appendix.

2 General description of the CTF3 preliminary phase

The general layout of the LPI complex before and after the modifications for the CTF3 preliminary stage is shown in Figure 1.

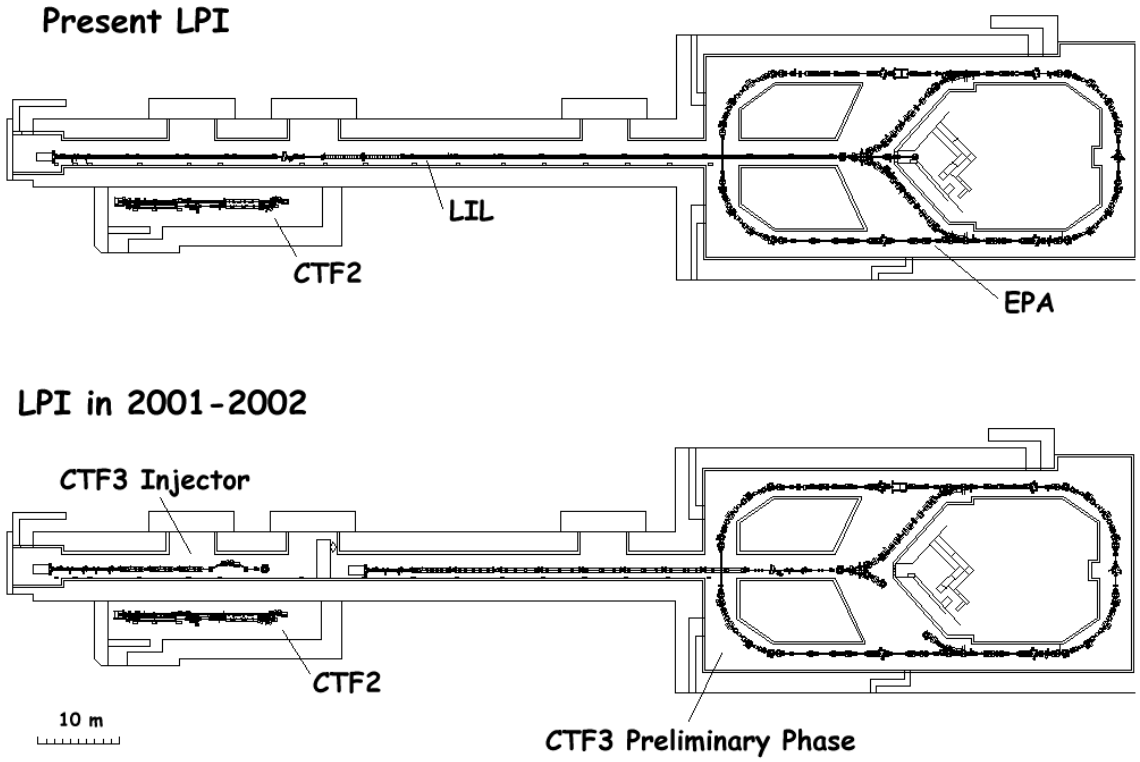

Figure 1: Layout of the LPI complex in the present configuration (top) and after the modifications for the CTF3 preliminary phase (bottom).

The first part of the LEP Injector Linac (LIL) will be dismantled and shielding blocks will be added, creating an independent area that can be used for component tests and later for the commissioning of the new CTF3 injector in 2002. A new gun [3] will be installed at the location of the present LIL positron capture region, followed by the existing LIL bunching system [4] which will be moved downstream. Eight of the sixteen accelerating structures of LIL will be removed, as well as the extraction lines to the PS complex and the positron injection line between LIL and the Electron Positron Accumulator (EPA) ring.

The new triode gun will provide a train of up to seven pulses. The nominal length of each pulse is 6.6 ns FWHM, and the pulses are spaced by 420 ns, corresponding to the EPA circumference. The gun will be operated with a nominal peak current of 1 A. The present bunching system, powered independently by a 30 MW klystron, will provide a 3 GHz bunched beam at 4 MeV. Each pulse will then consist of 20 bunches, each of them having a charge of 0.1 nC and a length of about 10 ps FWHM. A detailed description of the gun and of the bunching system is given in section 3.

The pulse train can be accelerated up to an energy of 380 MeV, using eight travelling wave accelerating structures, which are powered in groups of four by two 40 MW klystrons. In order to take into account an operational margin, a reference beam energy of 350 MeV is used in this note. The whole electron pulse train will be accelerated using a single RF pulse. Since the maximum train length ($\simeq 2.5$ μs) plus the cavities filling time ($\simeq 1.5$ μs) is not much shorter than the RF pulse length from the klystron ($\simeq 4.5$ μs), it has been decided not to use the present RF pulse compression system (LIPS, for LIL Power Saver). The beam parameters have been chosen in order to minimise the energy spread generated by beam-loading in the LIL structures, while still keeping a charge per bunch which is high enough to give a good resolution for the measurements of the beam time structure with a streak camera. The beam-loading parameter in LIL is 0.2 MeV/nC per structure. The resulting energy spread within each pulse is about 3 MeV. An additional energy difference of roughly 3 MeV will occur between the first two pulses, i.e. before the steady state is reached. The total energy spread of about 6 MeV is within the EPA full acceptance ($\pm 1\%$). It can nevertheless be reduced by a factor of two by delayed RF filling of the structure, or by dumping the first two pulses in the train (out of seven). For the frequency multiplication test, one needs at most five pulses. The linac optics has to be adapted to this new layout. The last two LIL accelerating structures will be removed and replaced by a matching section to the injection line. Apart from the new gun, no new equipment is needed in the linac and only a re-arrangement of the existing components is required. Some details on the new linac optics and on the matching region are given in section 4.

The present transfer line from LIL to EPA is achromatic in both planes. It must be noted that, in addition to the main horizontal bending magnets, the line contains two vertical dipoles with a small bending angle, since the heights of LIL and EPA differ by 15 cm in order to allow injection from the inside of the ring. However, the line must also be made isochronous, in order to preserve the bunch length from the linac to the ring. This is essential for the combination process, for which short bunches ($\leq$ 15 ps FWHM) are needed (see section 7). Furthermore, the line has to be re-matched to the new ring lattice. A new optics has been found, which satisfies the requirements of the CTF3 preliminary phase. Two quadrupoles must be added to the present layout, and some of the existing quadrupoles must be moved. All quadrupoles in the transfer line will be fed by independent power supplies. However, the overall geometry of the line is preserved, such that no major hardware modifications are needed. The quadrupoles and the power supplies from the dismantled beam lines can be re-used in the new line. Its design is presented in section 5.

The lattice of EPA will be modified to make the ring isochronous and thus to preserve the bunch length and spacing during the combination process (up to five turns). In a first isochronicity test performed in the EPA ring, the capability to control and measure the momentum compaction to the level required for the preliminary phase of CTF3 has been demonstrated [5]. In this experiment, the isochronous lattice was obtained by changing the strength of the existing quadrupole families. However, the dispersion was not vanishing in the long straight sections and the transfer line was badly matched to the ring, causing beam losses in the first few turns. Since the available aperture will be further reduced when the RF deflectors for the new injection scheme are installed, a

different optics had to be found. In the new isochronous lattice, the dispersion vanishes in the long straight sections. It requires the displacement of four quadrupoles and the decoupling of three out of the six existing quadrupole families. This new lattice of EPA is discussed in section 6.

Two transverse RF deflectors will be used instead of the present fast injection kickers. They will create a time-dependent closed bump of the reference orbit, allowing the interleaving of three to five bunch trains. More details are given in Figure 2 for a frequency multiplication factor of four. The bunch combination process requires:

$$C = n\lambda_0 \pm \lambda_0/N \tag{1}$$

where n is an integer, C is the ring circumference, N is the combination factor and λ_0 is the RF wavelength in the deflectors and the linac.

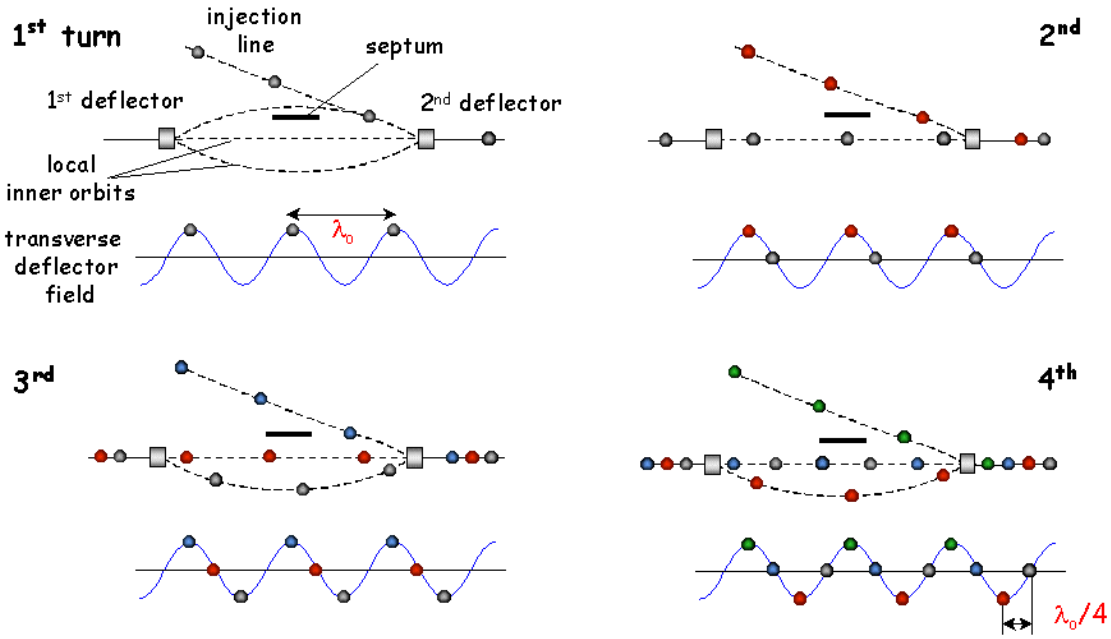

Figure 2: Schematic description of the injection by RF deflectors, for a bunch combination factor of four:
1) When the first train arrives, all of its bunches are deflected by the second deflector on the equilibrium orbit.
2) After one turn the bunches of the first train arrive in the deflectors at the zero-crossing of the RF field, and stay on the equilibrium orbit. The second train is injected into the ring.
3) The first train bunches are kicked inside the ring, the second train bunches arrive at the zero-crossing, and the third train is injected.
4) The first train bunches arrive again at the zero-crossing, the second train bunches are kicked in the inner orbit, the third train bunches are also at the zero crossing and the fourth train is injected. The four trains are now combined in one single train and the initial bunch spacing is reduced by a factor of four.

Combination factors of three, four and five will be tested in the preliminary phase of CTF3. The whole range of combination factors can be explored by changing the frequency of LIL and of the RF deflectors by ± 150 kHz. The frequency will be changed in the RF source at low level (before the klystrons), the bandwidth of the klystrons being wide enough to cover this range. The accelerating structures and the deflectors will be tuned in operation by varying their temperature by ± 3°C, in order to follow the change of the RF frequency. Recent measurements have shown that this can be done in the linac [6]. The RF deflectors are travelling wave iris-loaded structures. They have been used in the past to measure the bunch length in LIL [7]. They will be powered by one of the existing 30 MW klystrons and a power of about 7 MW is needed in each of them to obtain the nominal deflecting angle of 4.5 mrad at 350 MeV. The fast injection kickers will be kept in the ring to allow conventional single-turn injection. They will be used during commissioning, in order to check the ring optics prior to the installation of the RF deflectors. Also, one of the positron injection kickers, located at the opposite side of the ring, will remain in place and will be used to extract the circulating beam to a dump, located at the end of the present positron injection line. More details on the injection process and the RF deflectors are given in section 7.

A tracking with realistic longitudinal and transverse distributions for the particles in the beam has been performed in the transfer line and the EPA ring, in order to check the stability of the new optics when higher order effects are included. The results of this tracking are presented in section 8. In section 9, we briefly discuss the issue of the beam steering in the CTF3 preliminary phase. Finally, a summary and some conclusions are given in section 10.

3 The LIL front-end

The LIL front-end consists of a thermionic gun, a pre-buncher, a buncher, a matching section and beam diagnostics, as shown in Figure 3.

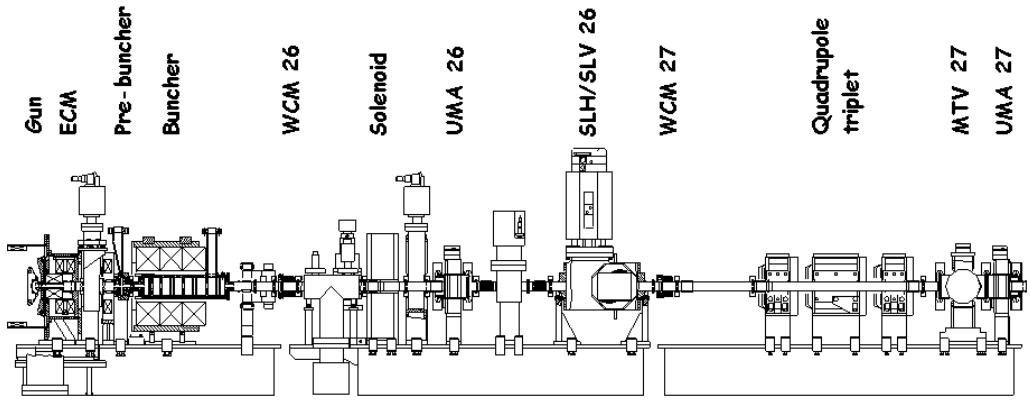

Figure 3: Layout of the LIL front-end.

3.1 The thermionic gun

For the CTF3 preliminary phase, only the existing LIL thermionic gun will be removed and replaced by a new thermionic gun. In order to simulate the beam dynamics in this gun, the EGUN code [8] was used, and it has been possible to obtain the required beam characteristics at the exit of the gun [9]. Figure 4 shows the beam envelopes from a 0.5 cm^2 cathode operating at 90 kV and 1 A, and with a hole of 10 mm (diameter) in the anode.

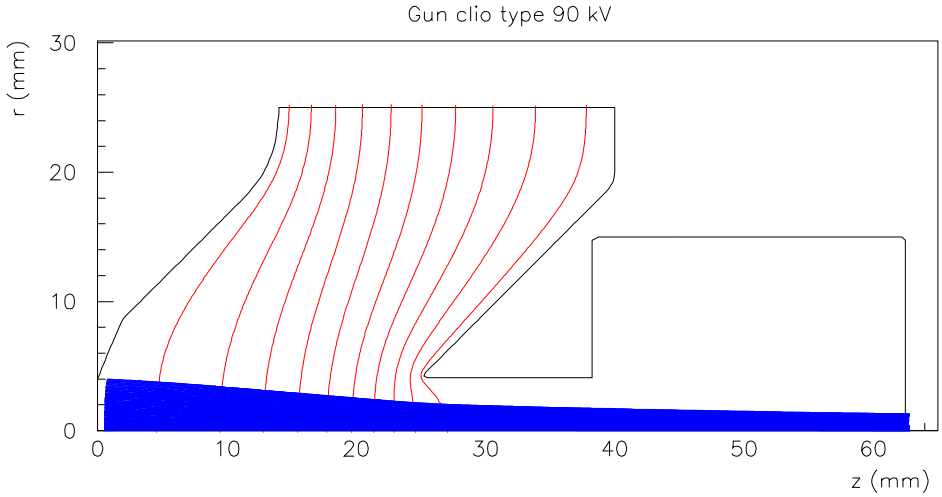

Figure 4: Beam envelopes (dark area) from EGUN simulations. The vertical lines between the anode and the cathode are the equipotential lines.

The existing gun of LIL is not adapted to the new requirements, since it has been designed for a current of 15 A, with no possibility to generate seven pulses spaced by several hundreds nanoseconds (in the CTF3 preliminary phase, the pulses must be spaced by 420 ns, which corresponds to EPA circumference). Therefore, a collaboration with the LAL institute has been set-up [10]. The new thermionic gun is a copy of an existing gun [11] which is used in the CLIO machine [12]. It produces a train of up to seven pulses with a repetition rate of 50 Hz. There are 20 electrons bunches per pulse, which means that the nominal length of each pulse is 6.6 ns FWHM. However, it can be varied between 4 and 10 ns, depending on how many electron bunches are in the pulse. The main characteristics of the CLIO gun are given in Table 1.

Element	Value	Unit
Voltage	90	kV
Voltage (conditioning)	100	kV
Current	2	A
Train length	2.6	μs
Pulse length	$4 \rightarrow 10$	ns
Rise time	< 2	ns
Jitter (over 420 ns)	$< \pm 0.3$	ns
Voltage stability	0.1	%
Normalized total emittance	< 15	mm.mrad
Repetition rate	50	Hz

Table 1: Main characteristics of the CLIO gun.

3.2 The bunching system

The present bunching system of LIL, composed of a single-cell pre-buncher and a standing wave buncher, will be used. Both operate at a frequency of 2.99855 GHz, which corresponds to a wavelength $\lambda_0 = 0.099979$ m.

The pre-buncher is a 15 mm long pill-box cavity and the buncher is a 341 mm long $2\pi/3$ standing wave structure [13]. In order to take into account the variation of the beam energy, the first cells of the buncher have different lengths. The buncher is a triperiodic structure working in standing wave mode, with three different periods: 0.92 λ_0, 0.98 λ_0 and λ_0. The distance of 100 mm between the pre-buncher and the buncher was optimised for a current of 3 A and a beam energy of 80 keV [14]. However, the nominal current is equal to 1 A in the CTF3 preliminary phase. The bunching efficiency can be optimised again by tuning the amplitude and the phase of the pre-buncher and the buncher.

No new beam dynamics simulations with PARMELA [15] were performed for the CTF3 preliminary phase. In the present situation, the current is lower and the voltage is slightly higher, so we do not expect any dramatic changes for the beam dynamics regarding the bunching system. This latter will be powered by a 30 MW klystron (MDK25) but only 4 MW are necessary. The beam energy at the output of the buncher is about 4 MeV.

The distance ℓ between the exit of the buncher and the first accelerating section (ACS27) is an important parameter. It was optimised in order to minimise the bunch length at the entrance of the first accelerating section. In the simulations, the choice of the phase for the buncher leads to an energy of 3.8 MeV ($\beta = 0.9929$) for the reference particle. In a bunch with a RF phase extension of 16° (or a total bunch length of 14.8 ps), a particle in the tail has an energy of 4.1 MeV ($\beta = 0.9938$). Therefore, $\Delta\beta/\beta = 0.1\%$. The electrons are not yet completely relativistic and the bunch length could be further reduced. When $\ell = 3.5$ m, a RF phase extension of 20° (18.5 ps) is compressed down to 16° (14.8 ps). Some measurements were performed with a RF deflecting cavity in 1990 [7] and gave 14 ps FWHM for the bunch length at a current of 3 A. Recent measurements, based on the energy spectrum analysis at 200 MeV, were also performed at a lower current and they gave 7 to 8 ps FWHM [16, 17].

Table 2 summarizes the main parameters of the injector for the CTF3 preliminary phase.

Element	Value	Unit
RF frequency	2.99855	GHz
RF wavelength	0.099979	m
Nominal gun voltage	90	kV
Maximum gun voltage	100	kV
Nominal gun current	1	A
Maximum gun current	2	A
Repetition rate	50	Hz
Distance from pre-buncher to buncher	100	mm
Pre-buncher voltage	47	kV
Pre-buncher accelerating gradient	1.3	MV/m
Buncher accelerating gradient	16	MV/m
Available RF power	30	MW
Temperature of the bunching system	30	°C
Beam energy	4	MeV
Distance from buncher to ACS27	3.5	m
Rms normalized beam emittance	40	mm.mrad
Bunch length (FWHM)	10	ps
Bunch charge	0.1	nC
Number of bunches	20	-
Number of pulses	7	-

Table 2: Main parameters of the new LIL injector.

3.3 The front-end matching section

In order to control the transverse beam dynamics, one solenoid and one quadrupole triplet are implemented. The optimisation of their settings was done with the TRANSPORT code [18]. Since the new conditions are very similar to the previous ones, it is proposed to keep the same matching section before the entrance of the linac for the CTF3 preliminary phase. The solenoid and the quadrupole triplet have independant power supplies, which

means four independent parameters to play with in the transverse phase space. Therefore, small variations of the initial conditions can be compensated by an optimisation of the matching conditions.

3.4 Beam instrumentation

The beam instrumentation used in the front-end is shown in Figure 3. A capacitive electrode (ECM), located just downstream the anode, allows to measure the beam current before the bunching system. A Wall Current Monitor (WCM26) measures the beam current at the exit of the bunching system. The ratio of the currents measured in WCM26 and ECM gives the bunching efficiency. The slits SLH26 and SLV26 are used for machine development. The Beam Position Monitors UMA26 and UMA27 [19] allow to check the transfer efficiency of the matching section and to align the beam in the first accelerating structure. They are also used to calibrate the WCMs. Finally a TV Monitor with the scintillator screen (MTV27) allows to check easily the presence of the beam and to get an estimate of the transverse beam sizes. On the existing front-end, the Transition-Cherenkov Monitor TCM 11 [20, 21] will be removed and it will be installed in the matching section at the end of the linac (see section 4.5).

4 The linac and the matching section

4.1 Reference lattice parameters near the entrance of the linac

Because of the modifications of the front-end, a new linac optics adapted to the new layout had to be studied. For this purpose, reference values of the Twiss parameters are needed near the end of the injector. Figure 5 shows the layout of the first sections of the linac in the present situation and during the CTF3 preliminary phase.

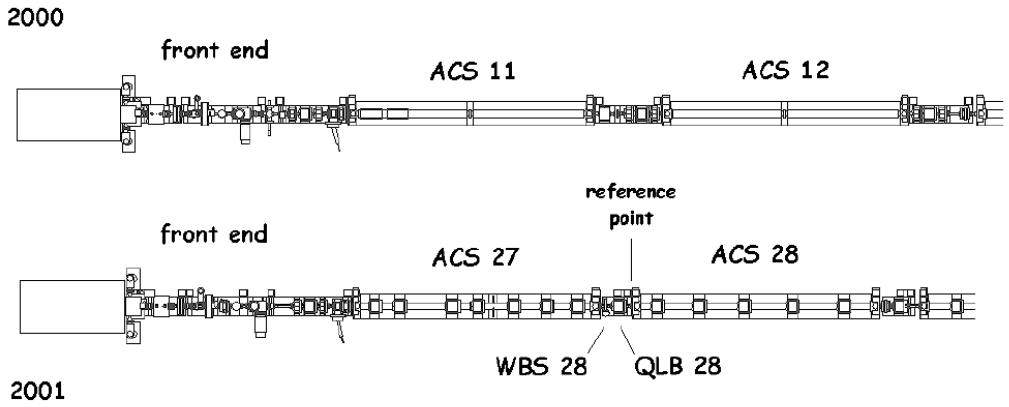

Figure 5: Layout of the front-end and the first sections of LIL in the present situation (top) and during the CTF3 preliminary phase (bottom).

Since it is difficult to simulate the RF focusing in the accelerating sections at low energy ($E \simeq 4$ MeV at the exit of the buncher), our reference point will stand just upstream ACS28. In the following, we assume that the beam properties at the end of the new front-end remain the same as in the present situation (all quadrupoles on ACS27, as well as QLB28, should thus be switched off). However, during the commissioning of the new linac, the values of the Twiss parameters just upstream ACS28 may slightly differ from what is used in this note. If necessary, the quadrupoles surrounding ACS27, as well as the triplet in the front-end, can be used to improve the matching between the exit of the front-end and the entrance of ACS28. The beam parameters have already been measured just upstream the present LIL positron capture region [16, 17]. In the existing layout, the beam properties at the entrance of ACS12 can be derived from this measurement. For this purpose, one needs to know the transfer matrix between the entrance of ACS12 and the measurement point, which is easily calculated by the MAD program [22]. Since we assumed that the beam properties at the end of the new front-end should be the same as in the present situation, the emittance and the Twiss parameters that we derive from the method described here can be used as a reference:

- the normalized rms emittance is 40 π mm.mrad for both the horizontal and the vertical phase spaces, and the energy before ACS28 is about 47 MeV,
- $\beta_x = 8.7$ m and $\alpha_x = +0.05$,
- $\beta_y = 11.9$ m and $\alpha_y = -0.22$.

4.2 New linac optics

In order to reach an energy of 350 MeV in the EPA ring, each of the eight accelerating structures of LIL must ensure an energy gain $\Delta E \simeq 43$ MeV. Since the LIL accelerating structures are surrounded by quadrupoles, a special treatment is necessary. In the optics calculations with MAD, the behaviour of these quadrupoles is simulated by the following sequence: acceleration up to the center of the quadrupole, drift in the backward direction down to the entrance of the quadrupole, quadrupole, drift in the backward direction down to the center of the quadrupole, acceleration up to the exit of the quadrupole. The RF focusing is taken into account in the simulation of the accelerating structures with MAD, which is not the case in TRANSPORT (however, the differences between the results given by these two codes are small).

For simplicity, none of the existing quadrupoles presently installed on LIL is moved (see Figure 6), except in the matching section which starts just downstream ACS34. In order to ensure a good beam transport until the end of the linac, their currents must be significantly lowered compared to what they are now, and all quadrupoles of the QNFA family, as well as the three first quadrupoles of ACS27 and QLB28, can be switched off. The maximum values of the β-functions along the linac are about 20 m, while β_x and β_y reach a few hundred meters in the current situation. Also, we noticed that, when varying slightly the initial conditions and some of the lattice parameters in the simulation, no significant changes of the beam properties are observed.

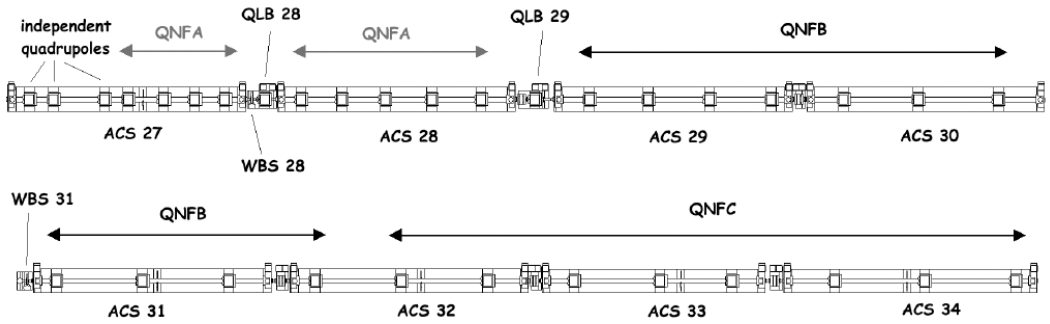

Figure 6: Layout of the linac between the front-end and the matching section, showing the various quadrupole families.

4.3 Design of the matching section

Between the end of ACS34 and the transfer line to EPA, a matching section will be installed instead of the present accelerating structures ACS35 and ACS36. Its layout is shown in Figure 7. The Twiss parameters at the end of the linac are imposed by the optics in the EPA ring and the transfer line, which must fulfill some specific conditions (see sections 5 and 6 for details). At the point referred to as zero, one must have:

- $\beta_x = 76.4$ m and $\alpha_x = +29.4$,
- $\beta_y = 39.1$ m and $\alpha_y = +10.2$.

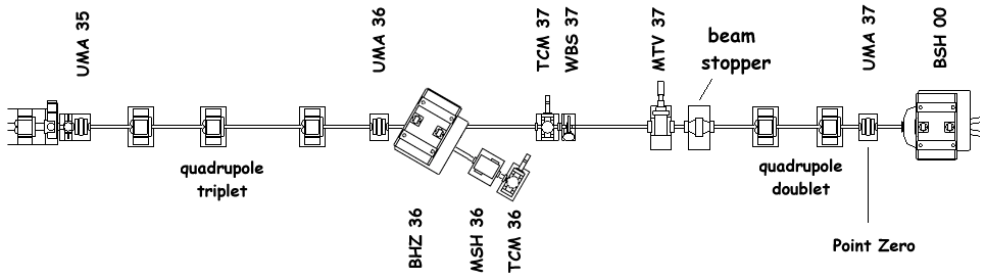

Figure 7: Schematic layout of the matching section located between the linac and the transfer line to EPA.

For the design of the matching section, the values of the Twiss parameters at the exit of ACS34, as derived from the calculation done for the linac, are used for reference. A good matching can easily be obtained by optimizing the normalized gradient and the position of each of the five quadrupoles.

4.4 Transverse beam dynamics in the new linac and in the matching section

Figure 8 shows the β-functions that we use as a reference, between the entrance of ACS28 and the point referred to as zero, when the settings of the various quadrupoles in the linac and the matching section are the ones displayed in Table 3.

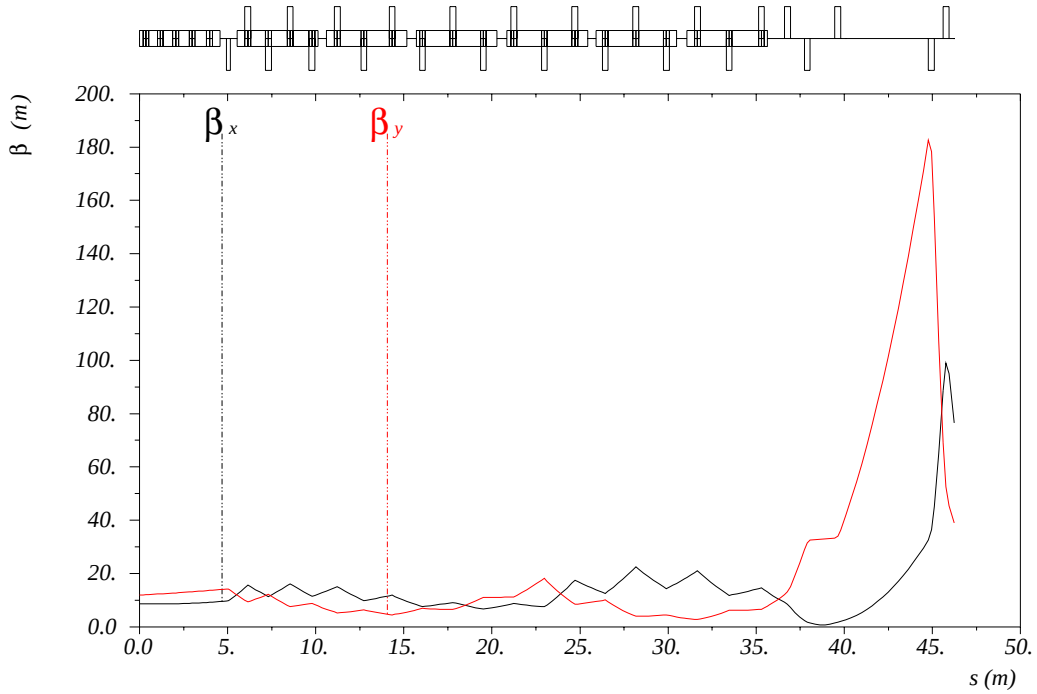

Figure 8: Evolution of the β-functions along the linac and the matching section.

Name	Length (mm)	Current (A)	K (m^{-2})	Distance (m)
WL.QNM271	328	0	0	0.321
WL.QNM272	328	0	0	0.801
WL.QNM273	328	0	0	1.824
WL.QNF271	328	0	0	2.304
WL.QNF272	328	0	0	3.010
WL.QNF273	328	0	0	3.635
WL.QNF274	328	0	0	4.232
WL.QLB28	220	0	0	5.031
WL.QNF281	328	0	0	5.767
WL.QNF282	328	0	0	6.581
WL.QNF283	328	0	0	7.451
WL.QNF284	328	0	0	8.381
WL.QNF285	328	0	0	9.374
WL.QLB29	220	-5.0	-0.926	10.446
WL.QNF291	328	+20.0	+0.996	11.541
WL.QNF292	328	-20.0	-0.894	12.712
WL.QNF293	328	+20.0	+0.806	13.946
WL.QNF294	328	-20.0	-0.734	15.182
WL.QNF301	328	+20.0	+0.686	16.626
WL.QNF302	328	-20.0	-0.623	18.126
WL.QNF303	328	+20.0	+0.567	19.732
WL.QNF311	328	-20.0	-0.532	21.457
WL.QNF312	328	+20.0	+0.488	23.184
WL.QNF313	328	-20.0	-0.450	24.914
WL.QNF321	328	+20.0	+0.428	26.644
WL.QNF322	328	-50.0	-0.976	28.374
WL.QNF323	328	+50.0	+0.914	30.104
WL.QNF331	328	-50.0	-0.874	31.834
WL.QNF332	328	+50.0	+0.823	33.564
WL.QNF333	328	-50.0	-0.778	35.304
WL.QNF341	328	+50.0	+0.751	37.064
WL.QNF342	328	-50.0	-0.712	38.864
WL.QNF343	328	+50.0	+0.676	40.692
WL.QNF351	328	+70.0	+0.960	42.174
WL.QNF352	328	-72.7	-0.997	43.302
WL.QNF361	328	+54.6	+0.749	45.030
WL.QNF362	328	-162.9	-2.233	50.344
WL.QNM363	328	+198.1	+2.716	51.172
Point zero	-	-	-	51.636

Table 3: Central positions (with respect to the entrance of ACS27) and properties of the quadrupoles in the linac and in the matching section. Positive (respectively negative) currents and normalized gradients stand for focusing (respectively defocusing) quadrupoles. The beam energy is 4 MeV at the beginning of the linac and 350 MeV at the end of the linac, i.e. in the matching section.

One should be aware that, during the commissioning of the linac, the values obtained at the exit of ACS34 may be slightly different from what we have calculated here. For instance, one should not take for granted the accuracy of the simulation of the accelerating structures when a quadrupole and a constant electric field are superposed (another method based on an analytical description of this system is under investigation). Consequently, some flexibility must be kept for the matching section (however, as already mentioned, the beam properties are not strongly affected by small changes in the lattice). During the commissioning of the machine, the accurate measurement of the beam parameters at the entrance of the matching section will be important, in order to further find the best matching conditions with the simulation codes.

4.5 Beam instrumentation in the linac and the matching section

Wherever possible, it has been chosen to keep in place the present beam instrumentation in the linac.

UMAs are placed between the accelerating structures, except at two locations, where Wire Beam Scanners (WBS) are or will be installed. The use of UMAs for beam steering will be discussed in section 9. Between ACS27 and ACS28, WBS28 is already installed. Another Wire Beam Scanner (WBS31) will be recuperated and placed between ACS30 and ACS31, where the present UMA31 is. These instruments will allow the measurement of the transverse beam characteristics (emittance and Twiss parameters) through quadrupole scans. In particular, using WBS28 and WBS31, it will be possible to check the beam parameters at the exit of the front-end and at the linac reference point upstream ACS28, respectively.

The matching section will be instrumented in order to provide a full characterization of the beam before injection into EPA (see Figure 7). The two UMAs at the beginning and at the end of the matching section (UMA35 and UMA37) will be kept at their present location, while the third UMA (currently located between ACS35 and ACS36) will be slightly displaced. A Wire Beam Scanner (WBS37) and a Transition-Cherenkov Monitor (TCM37) will be placed in the straight line. The WBS will allow the determination of the transverse beam parameters at the entrance of the matching section. In the TCM, a Transition radiation screen or a Cherenkov screen can be alternatively put in the beam path. In conjunction with an image frame grabbing system and digital treatment, the TCM can be used for the determination of the transverse beam parameters and it will provide a way to cross-check the results of the WBS. The aim is to eventually use the TCM routinely for emittance and Twiss parameters measurements, using an automated program derived from the one currently in use in CTF2 [23], providing a much shorter measurement time with respect to the quadrupole scan with a WBS. A camera (MTV37) will complete the instrumentation of the straight beam line.

A dipole magnet (BHZ36), recuperated from a dismantled line, will be installed in the matching section in order to deflect the beam into a spectrometer line. The line will be equiped with a SEMgrid (MSH36) and a Transition-Cherenkov Monitor (TCM36). The nominal bending angle in BHZ36 will be 35°. Since the dispersion at the MSH location will be about 0.75 m, and since the SEMgrid wires are spaced by 2 mm, the

energy resolution will be 0.3%. With 20 wires, the acceptance on the MSH36 screen will be about 5%. Assuming that β_x can be tuned down to 1 m in MSH36, with a rms normalized emittance of 40 π mm.mrad, the rms beam size for a monochromatic beam should be around 0.2 mm and should thus not limit the spectrometer resolution.

An optical transport line will also be installed, in order to bring the light generated in TCM36 and TCM37 up to the streak camera laboratory. Therefore, TCM37 could be used for time-resolved measurements of the transverse beam parameters which can be useful, e.g. to study chromatic aberrations in the linac. The use of the streak camera with TCM36 will allow a time-resolved measurement of the beam energy spectrum. Using TCM36, where the dispersion will be about 1 m, we should be able to resolve pulse-to-pulse and bunch-to-bunch energy variations due to beam-loading.

5 The injection line between the linac and EPA

The design of the transfer line between the linac and the EPA ring has to meet several requirements for the CTF3 preliminary phase. The main modification consists in having an isochronous lattice, in order to avoid direct bunch lengthening. Also, the transverse Twiss functions have to be matched at both ends of the line, as well as the horizontal and vertical dispersion functions and their derivatives. On top of that, in order to keep chromatic effects at a low level, small β-functions are required, well under the present values of a few kilometers. From a general point of view, the requirements on the new injection line are more stringent than for the existing one: in particular, transverse and dispersion matching must be very precise due to the aperture restriction from the RF deflectors in the ring (see section 7) and because of the achromaticity condition. This differs from the existing transfer line, where the tolerances on injection are relaxed because of the damping process in the accumulation ring used for lepton production.

5.1 Physics requirements

To first order, the evolution of the bunch length through the transfer line is controlled by the coefficients of the linear 6×6 transfer matrix R. When neglecting vertical dispersion, which is indeed much smaller than the horizontal dispersion in the transfer line, the path length difference of a given particle with a relative momentum difference $\frac{\Delta p}{p}$ with respect to the reference particle is given by:

$$c\Delta t = R_{51}x + R_{52}x' + R_{56}\frac{\Delta p}{p}. \tag{2}$$

Here (x,x') refers to the usual horizontal phase space at the entrance of the line and, for a reference path $\mathcal{L}$ along the line, the matrix coefficients are defined by:

$$R_{51} = \int_{\mathcal{L}} \frac{C}{\rho}\, ds \quad , \quad R_{52} = \int_{\mathcal{L}} \frac{S}{\rho}\, ds \quad , \quad R_{56} = \int_{\mathcal{L}} \frac{D}{\rho}\, ds \tag{3}$$

where ρ is the bending radius, C and S are the cosine-like and sine-like principal solutions of Hill's equation of motion, and D is the horizontal dispersion.

As for the rms bunch length σ_ℓ, the following equation can be obtained:

$$\sigma_{\ell f}^2 = \sigma_{\ell i}^2 + (R_{56}\sigma_E)^2 + \epsilon_{xi}(R_{51}^2\beta_{xi} - 2R_{51}R_{52}\alpha_{xi} + R_{52}^2\gamma_{xi}). \tag{4}$$

In this equation, σ_E is the rms energy spread. The subscript i refers to the entrance of the transfer line, while the subscript f can refer to any point downstream.

The matching of the horizontal dispersion and its first derivative at both ends of the transfer line requires a first order achromat: $D_{xi} = D'_{xi} = 0$ are the values of the dispersion and its derivative at the entrance of the line (end of the linac) while $D_{xf} = D'_{xf} = 0$ are their values at the end of the line (injection point in the EPA ring). For such boundary conditions, it can be shown that R_{51} and R_{52} vanish:

$$\begin{cases} D_{xi} = D'_{xi} = 0 \\ D_{xf} = D'_{xf} = 0 \end{cases} \Longrightarrow R_{51} = R_{52} = 0. \tag{5}$$

From equations (2) and (4), the last condition to fulfill is the first-order isochronicity, i.e. $R_{56} \simeq 0$. This requires the modification of the horizontal dispersion function along the transfer line, in order to force the ratio D/ρ to change sign, so that the third integral of equation (3) vanishes over the total path length. The new design of the transfer line was mainly driven by this condition, and by the fact that the new layout should only generate minor modifications to the existing hardware.

5.2 Characteristics of the new transfer line

In the new configuration, the dipole magnets are neither moved nor changed compared to the present situation of the transfer line. However, two new focusing quadrupoles are needed in order to control the value of R_{56}: one upstream the dipole BHZ10, near the beginning of the line, and the other one downstream the dipole BHZ30, just before the first injection septum. The positions and the normalized gradients of the existing quadrupoles are modified according to the needs. For instance, four out of five quadrupoles in the central straight part of the line must be moved and all will be fed by independent power supplies.

The modifications of the layout and of the optics for the new transfer line are summarized in Figure 9 and Table 4. In this solution, all quadrupoles are used in a global way to cope with all constraints: the small R_{56} factor, the horizontal and vertical dispersion matching and the transverse Twiss parameters behaviour. A different optics was studied, with no dispersion in the central straight part of the transfer line. This had the advantage of partially decoupling the transverse and longitudinal matchings, but it was abandoned, because it is not feasible with the existing hardware.

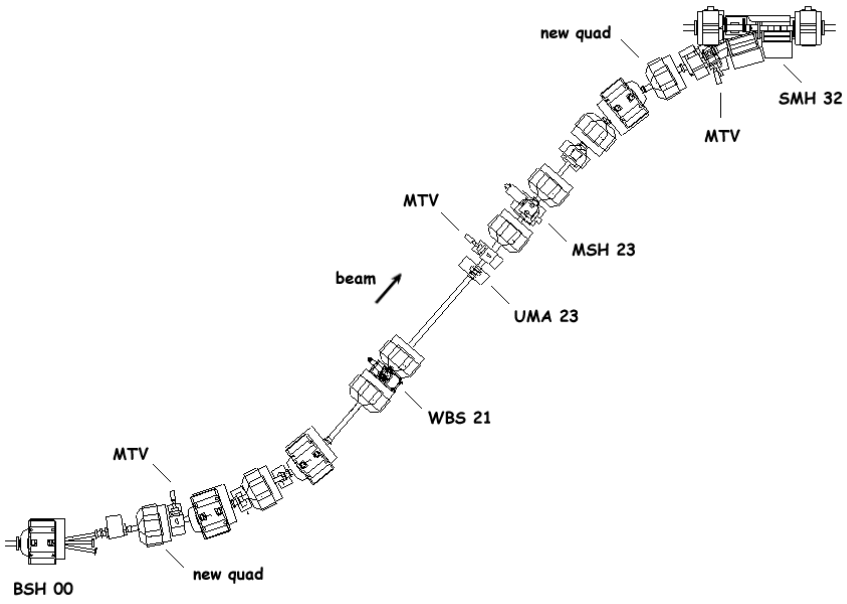

Figure 9: Layout of the modified transfer line.

Element	Angle (degrees)	Gradient (m^{-2})	Position (m)
HIE.BSH00	-9		1.077 (unchanged)
HIE.BVT00	+0.55 (vertical)		2.526 (unchanged)
HIE.QFW01		+4.360	3.263 (new)
HIE.BHZ10	-20		4.474 (unchanged)
HIE.QDW11		-4.360	5.578 (unchanged)
HIE.BHZ20	-20		6.724 (unchanged)
HIE.QFW21		+2.870	8.383 (moved)
HIE.QDW22		-2.948	9.258 (moved)
HIE.QFW23		+2.154	12.649 (moved)
HIE.QDW24		-3.040	13.975 (moved)
HIE.QFW25		+3.712	15.450 (unchanged)
HIE.BHZ30	+20		16.270 (unchanged)
HIE.QFW30		+3.980	17.291 (new)
HIE.BVT30	-0.55 (vertical)		17.918 (unchanged)
HIE.SMH31	+21.75		18.916 (unchanged)
HIE.SMH32	+7.25		19.619 (unchanged)

Table 4: Central positions (with respect to point zero) and properties of the magnetic elements in the new transfer line for the CTF3 preliminary phase. Positive (respectively negative) gradients stand for focusing (respectively defocusing) quadrupoles.

The Twiss functions of the new lattice are shown in Figure 10, while the dispersion functions are shown in Figure 11 (the vertical dispersion differs from zero because of the two vertical bending magnets used to match the LIL and EPA heights).

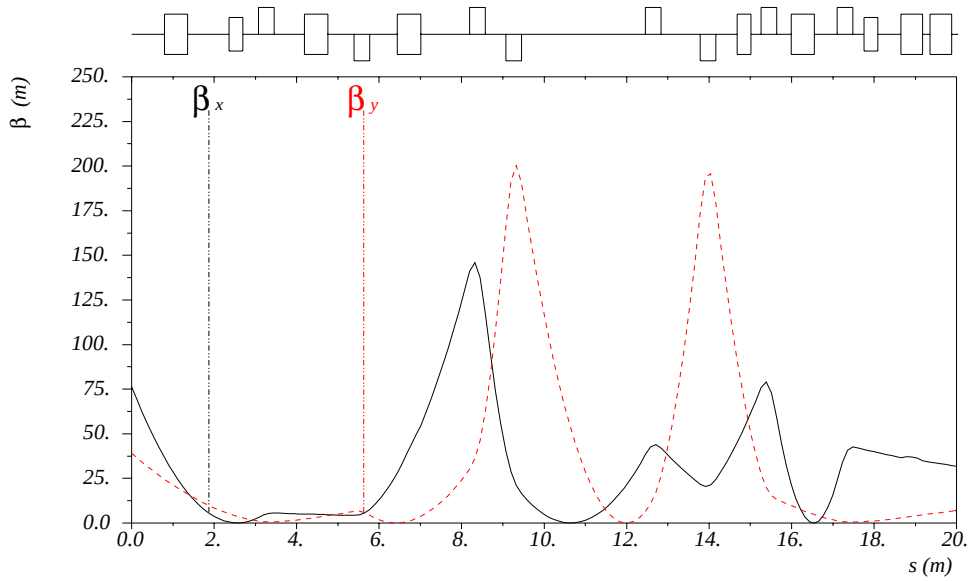

Figure 10: Horizontal and vertical β-functions along the transfer line between the linac (point zero) and the isochronous EPA ring (injection point).

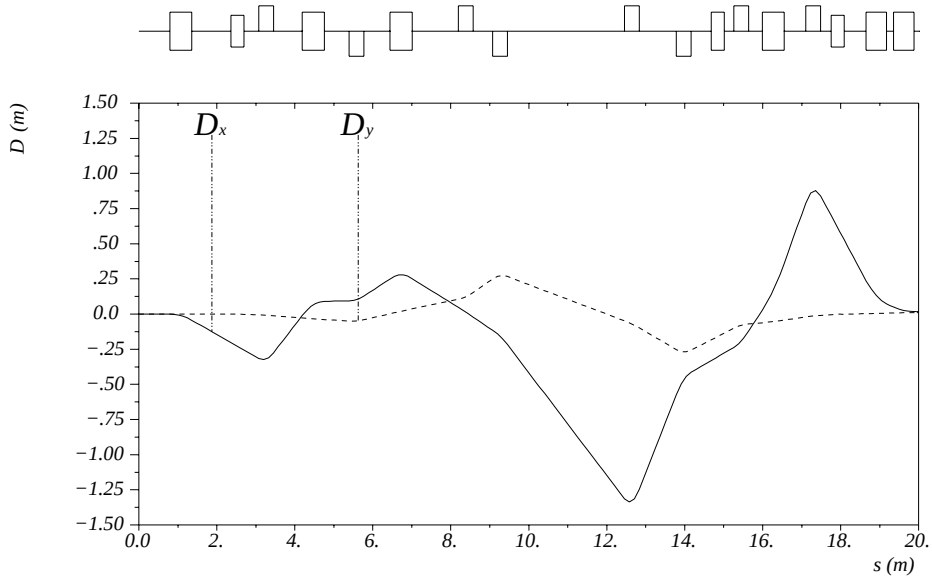

Figure 11: Horizontal and vertical dispersion functions along the transfer line between the linac (point zero) and the isochronous EPA ring (injection point).

This configuration allows a quasi-isochronous operation with $|R_{56}| \leq 10^{-2}$ m, compared to $R_{56} \simeq -1$ m before the transformation. Shown in Figure 12 is the variation of the path length with the relative momentum error in the transfer line.

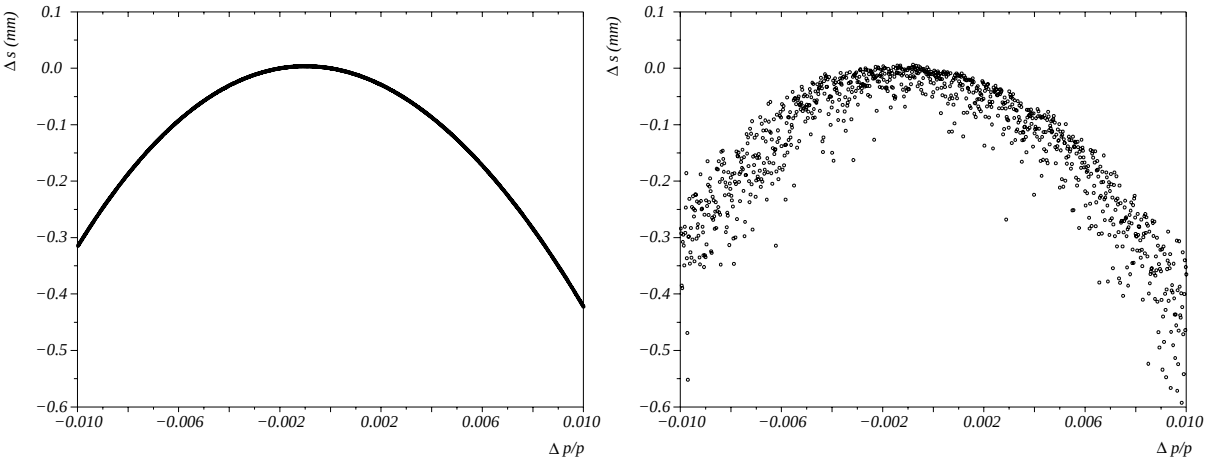

Figure 12: Variation of the path length with the relative momentum error in the transfer line. On the left-hand side of the figure, the tracking is done with a zero emittance and a momentum spread of ±1%. On the right-hand side, the normalized rms emittance of 40 π mm.mrad is included in both transverse planes.

This figure shows that the first order isochronocity is very small and that the dominant effect is the second order isochronicity. Such an effect is still acceptable and no corrections with sextupoles are needed. The effect of the emittance is shown on the right-hand side of the figure: it is visible but it remains small. As a consequence, no significant bunch

lengthening is observed between the entrance and the exit of the line. However, along the transfer line, the bunch length varies according to equation (4): it grows in the first bends, reaches a maximum in the central straight part of the line and then decreases in the last bends, following the value of R_{56}. Figure 13 shows the evolution of the bunch length as a function of the curvilinear abscisse in the transfer line.

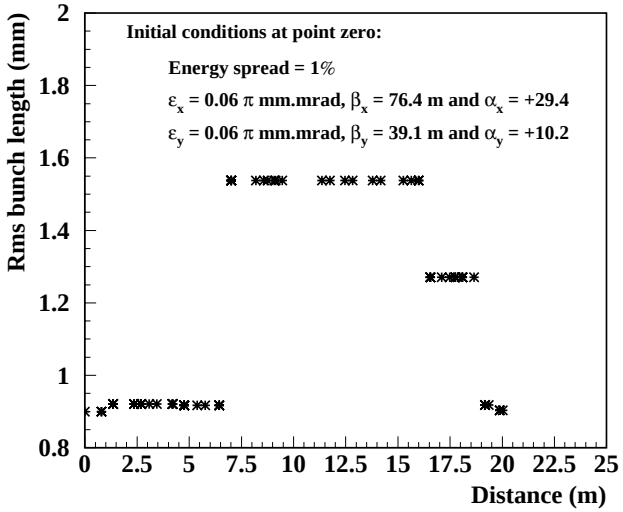

Figure 13: Evolution of the rms bunch length along the transfer line between the linac and the EPA isochronous ring. An initial rms bunch length σ_{li}=0.9 mm and an energy spread σ_E=1% are considered. Here, the emittance is 0.06 π mm.mrad (which corresponds to a rms normalized emittance of 40 π mm.mrad, since the beam energy is 350 MeV).

The beam properties in the transverse plane at the beginning of the transfer line are imposed by the values of the Twiss parameters needed to match the transfer line to the EPA ring. At the injection point (15 cm downstream the exit of SMH32), they are:

- $\beta_x = 31.2$ m and $\alpha_x = +2.2$,
- $\beta_y = 7.0$ m and $\alpha_y = -1.6$.

Therefore, knowing the transfer matrix of the new transfer line, the Twiss parameters needed at the end of the linac (point zero) can be derived. Their values are the ones which are used in section 4.3 and which are reported in Figure 13.

5.3 Beam diagnostics in the transfer line

The beam diagnostics elements of the transfer line are shown in Figure 9.

Three television cameras (MTV) are distributed along the line: the first one is located upstream BHZ10 in the first bending region, the second one is in the straight section upstream QFW23, and the last one is downstream BVT30, before the injection septa. These screens will help follow the beam through the injection line.

A WBS is located between the quadrupoles QFW21 and QDW22 in the straight section. In the proposed optics, this position corresponds to a zero-crossing region of the dispersion function with high values of the β-functions in the vertical and horizontal planes. This allows quadrupole scans so as to characterize the transverse behaviour of the beam and to make comparisons with the design optics.

A SEMgrid is also located downstream in the central straight part of the line, between the quadrupoles QFW23 and QDW24, in a region with high dispersion, in order to check the value of the dispersion and to measure the mean energy and the energy spread at this point.

6 The EPA ring with isochronous optics

6.1 Isochronous optics with the nominal EPA machine

The momentum compaction factor of the nominal EPA optics ($\alpha = 0.034$), combined with a momentum spread of $\pm 1\%$, does not allow the injected bunches to remain short enough after five turns for the purposes of the CTF3 tests. The path length differences between the particles with extreme momenta in the bunches exceed 80 mm per turn, which is too large by more than two orders of magnitude to preserve FWHM bunch lengths in the 10 ps range. In a first test in 1999, using existing magnets and cabling, the EPA optics was modified to yield $\alpha = 0$ [24, 25]. Using the chromaticity sextupoles, the path length could be controlled to within 0.035 mm per turn across the momentum range of the bunches, while keeping the horizontal and vertical chromaticities close to zero. Unfortunately, the dispersion could not be cancelled in the injection region with the existing quadrupole layout and powering. This resulted in a dispersion mismatch between the injection line and the ring, and the injection efficiency was smaller than with the nominal EPA optics. Equally, the single turn path lengths were modulated by this mismatch, thus perturbing the evolution of the bunch length over the first few turns.

6.2 Isochronous optics with the modified EPA ring

In the CTF3 preliminary phase, the constraint of being compatible with lepton production for LEP disappears and it will become possible to displace or reconfigure the quadrupole families. The proposed optics will limit the transverse beam sizes in the small aperture RF dipoles (see Figure 14). On top of small β_x and β_y values, this requires $D_x = 0$ in the injection straight sections.

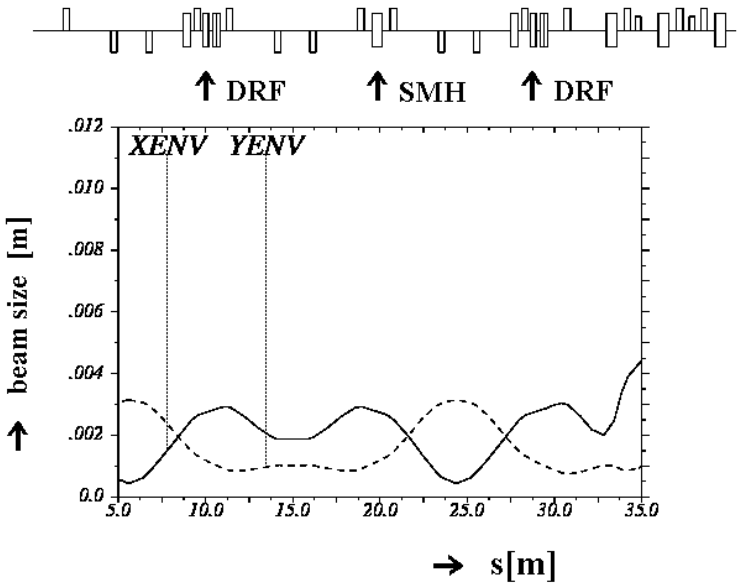

Figure 14: Horizontal and vertical beam sizes at 2σ. The rms normalized emittance is 40 π mm.mrad and $\sigma_E = 5.0 \times 10^{-3}$ in the injection area (the beam energy is 350 MeV). The arrows indicate the locations of the RF dipoles (left, right) and the septum (center).

With the new optics, the symmetry in each of the four arcs with respect to their center is abandoned. All six quadrupoles in each arc are now powered individually, increasing the number of arc quadrupole families from three to six. On the other hand, the symmetry of the ring with respect to the center of each of the four straight sections between the arcs is preserved. By choosing appropriate integer tune values, the required gradients could be kept at a moderate level, and the new isochronous optics can be achieved with the present magnets up to a beam energy of 400 MeV. The strengths of the quadrupoles in the long straight sections are unchanged, in order to keep the beam sizes and trajectories close to those of the nominal EPA optics. In order to better match the arc optics to the straight section optics, one quadrupole (QFWb) in each arc must be displaced by 1.85 m towards the long straight section. The new layout of one EPA arc is shown in Figure 15, while Table 5 gives the values of the normalized gradients of all quadrupoles in the proposed isochronous EPA ring.

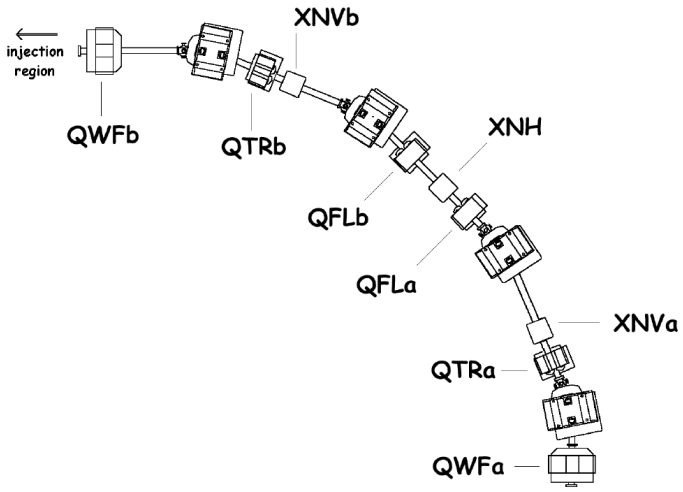

Figure 15: Layout of one EPA arc, showing the new locations of the quadrupoles and the sextupoles.

Quadrupole name	Normalized gradient (m^{-2})
HR.QFWa	+1.016
HR.QFWb	+0.571
HR.QFLa	+2.566
HR.QFLb	+0.305
HR.QTRa	+0.179
HR.QTRb	+1.078
HR.QFN	+0.566
HR.QDN	-0.569
HR.QFI	+0.534

Table 5: Normalized gradients of the quadrupoles for the EPA isochronous optics. Positive (respectively negative) gradients stand for focusing (respectively defocusing) quadrupoles.

Figure 16 shows the horizontal and the vertical β-functions, as well as the dispersion function, in one arc of the new isochronous EPA ring.

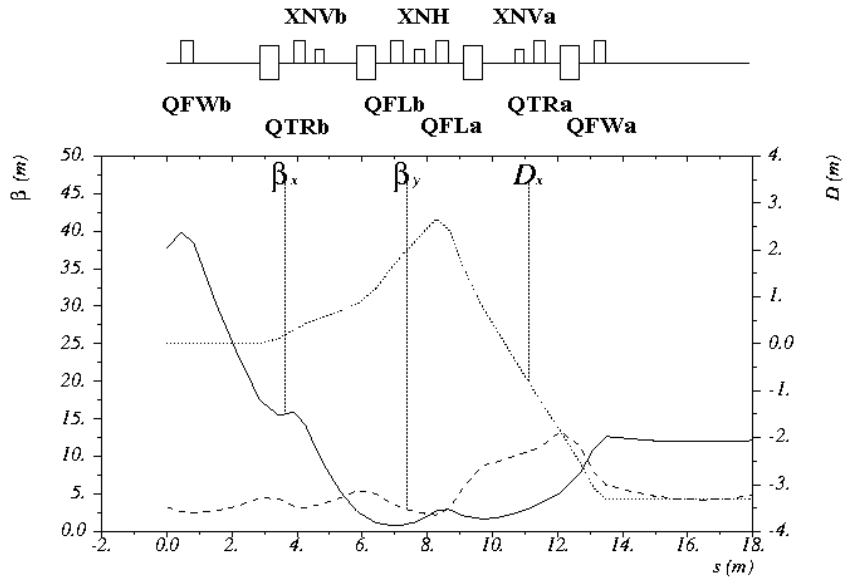

Figure 16: Lattice functions in one arc of the EPA ring. The names of the six quadrupole and the three sextupole families are shown.

In addition to the isochronous optics ($\alpha = 0$), another optics, with $\alpha = 0.034$, has been designed to be used during the commissioning of the new EPA ring. This latter optics will allow the RF system to keep a stored beam circulating for beam diagnostics purposes. In this case, the values of the normalized gradients of all quadrupoles are those given in Table 6.

Quadrupole name	Normalized gradient (m^{-2})
HR.QFWa	+1.471
HR.QFWb	+0.635
HR.QFLa	+2.550
HR.QFLb	-1.231
HR.QTRa	-0.273
HR.QTRb	+0.999
HR.QFN	+0.566
HR.QDN	-0.569
HR.QFI	+0.534

Table 6: Normalized gradients of the quadrupoles for the EPA non-isochronous optics. Positive (respectively negative) gradients stand for focusing (respectively defocusing) quadrupoles.

6.3 Change of the EPA circumference

The LIL machine has a nominal RF frequency of 2.99855 GHz, which corresponds to a wavelength $\lambda_0 = 0.099979$ m. The circumference of the present EPA ring (nominally 40 π m, confirmed by recent measurements [6]) is thus equal to 1256.9 λ_0. Bunch train recombination over three, four or five turns in EPA requires circumferences of 1256.666 λ_0, 1256.750 λ_0 or 1256.800 λ_0 respectively. To keep these three options open with the same ring layout, an average circumference value of 1256.73 nominal wavelengths has been chosen. The required reduction of the EPA circumference is thus equal to 0.17 λ_0, i.e. 17 mm. In order to switch between three, four or five turn recombination, the RF frequency will be slightly detuned.

6.4 Performances

The isochronous optics for EPA provides $D_x = 0$ in the two injection long straight sections (see Figure 16), but a non-zero horizontal dispersion in the two other straight sections. The transfer matrices between injection elements are the same as in the nominal machine. The beam sizes in the RF dipoles remain sufficiently small compared to their mechanical aperture (the smallest diameter is 21 mm).

The natural chromaticities of the new isochronous optics are comparable to those of the nominal EPA optics. Equally, the off-momentum path lengths can be controlled using the chromaticity sextupoles (now organised in three families instead of two) to within 0.5 mm per turn across the momentum range of the bunches, while keeping the chromaticities small (see Figures 17 and 18), as in the 1999 EPA optics [24]. Tracking over 1000 turns shows horizontal and vertical dynamic apertures around 15σ across the momentum range of the incoming beam.

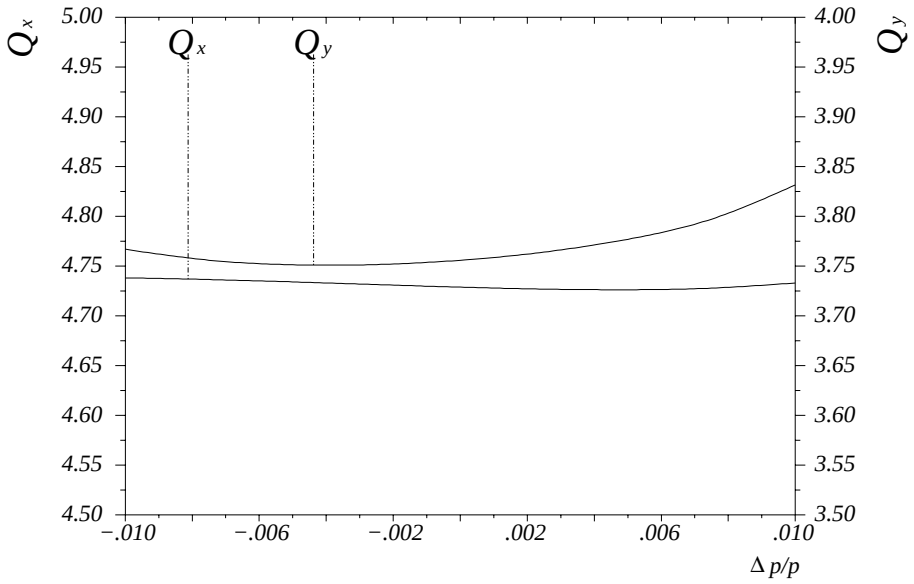

Figure 17: Horizontal and vertical tunes, versus the relative momentum error.

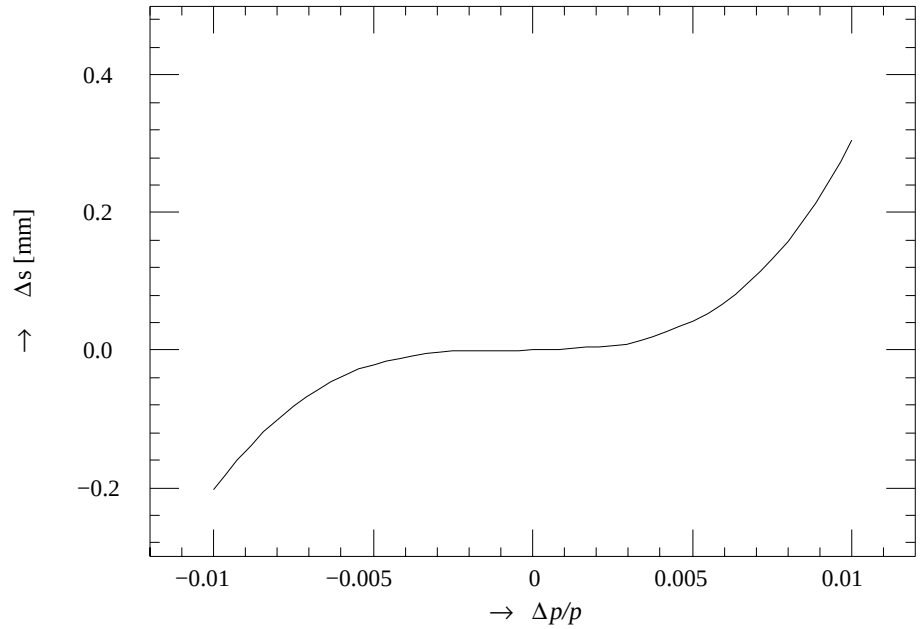

Figure 18: Variation of the one turn orbit length with the relative momentum error.

6.5 Beam diagnostics in the EPA ring

The existing instrumentation in EPA will be used in the preliminary phase of CTF3 without major modification, with the exception of WBS82. The only quadrupole (QFI82) located between the injection septum and WBS82 is too close to the Wire Beam Scanner, and can thus not be used to perform measurements on the incoming beam. A new location further downstream will be found for this device, so that WBS82 can be used to perform quadrupole scans at injection, enabling us to check the transverse matching of the injected beam to the EPA ring optics.

Furthermore, the existing optical lines used to transport the synchrotron radiation signal to the streak camera will be modified. Since positrons will no longer circulate in the EPA ring, the optical lines can be simplified: some semi-transparent elements can be dismantled, increasing the amount of light available. By using a moving mirror, part of this optical line can be made common with the optical lines used for TCM36 and TCM37, which are located in the matching section. It must be noted that the synchrotron light measurement with the streak camera is the main diagnostic tool available to observe the beam time structure in detail. As shown in previous tests in EPA [25], the precise tuning of the ring optics to isochronicity can be obtained rather easily by using the streak camera to observe the bunch length and distance over several turns. The streak camera measurement will also eventually provide the demonstration that the bunch combination process can indeed be achieved as planned.

More information on the Beam Position Monitors in EPA can be found in section 9.

7 Injection using RF deflectors

In order to achieve bunch frequency multiplication, the bunch trains are injected in the isochronous EPA using two RF deflectors which are placed in the ring with a betatron phase advance of π between them, so that they produce a time-dependent closed bump (see Figure 2 for details).

The present injection scheme is shown in Figure 19. It uses a pair of static dipoles (bumpers) to bring the orbit close to the septum and two fast kickers for the fast injection. The bumpers, as well as the kickers, have a phase advance of π between them. In 2001, two RF deflectors will be installed at the locations of the bumpers. The kickers will not be moved, while the bumpers will be slightly displaced. The RF deflectors, whose positions are also shown in Figure 19, will be used instead of the kickers for the bunch combination tests.

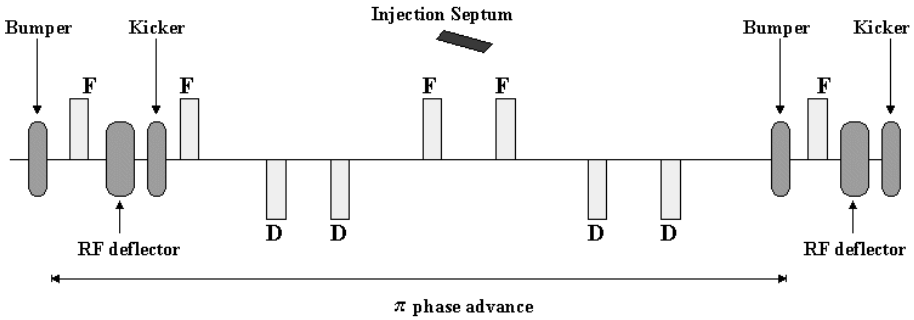

Figure 19: Schematic layout of the injection region (an arbitrary scale is used).

7.1 The RF deflectors

For the CTF3 preliminary phase, the RF deflectors are short, travelling wave, iris-loaded structures for which the fundamental mode is a deflecting mode, with a phase advance of $\pi/2$ per cell and a negative group velocity [26]. Each deflector has an overall length of 27 cm, with six regular cells (and the two couplers) and an iris diameter of 2.3 cm (2.1 cm in the coupler cells). In this type of cavity, the deflecting force is uniform in strength and direction over the aperture [27]. The voltage attenuation along the structure is characterized by the constant α and the deflection angle is given by:

$$\phi = \frac{\sqrt{ZP}}{E}\left(\frac{1-e^{-\alpha L}}{\alpha}\right) \tag{6}$$

where P is the input power, L is the total active length, E is the electron beam energy, and Z is the series impedance defined as:

$$Z = \frac{R}{Q}\frac{2\pi}{\lambda_0}\frac{1}{\beta_g} \tag{7}$$

where R is the shunt impedance, λ_0 is the RF wavelength, Q is the quality factor, and β_g is the normalized group velocity.

When using the parameters given in Table 7, a reference injection angle of 4.5 mrad is found for a 7 MW input power (the two couplers are considered as two active cells for the transverse deflection). The main drawback of the existing RF deflectors is their limited aperture. Therefore, new deflectors with a larger aperture, built by INFN Frascati, could possibly become available in 2002 [28].

Parameter	Symbol	Value	Unit
Frequency	ν	2.998	GHz
Number of cells	N_c	6+2	
Dephasing/cell		$\pi/2$	
Opening	$2a$	2.3	cm
Diameter	$2b$	11.9	cm
Cell length	d	2.5	cm
Active length	L	20	cm
Overall length	L_d	27	cm
Normalized group velocity	β_g	-0.0189	
Quality-factor	Q	1.281×10^4	
Shunt impedance	R	3.389×10^7	$\Omega.\mathrm{m}^{-1}$
Series impedance	Z	8.797×10^6	$\Omega.\mathrm{m}^{-2}$
Voltage attenuation	α	0.13	m^{-1}
Input power	P	7	MW
Deflection angle	ϕ	4.5	mrad

Table 7: Main parameters of the RF deflectors [29].

7.2 Injection scheme

The angle required for injection is given by both the geometry of the injection region and the optics. If μ_x is the horizontal phase advance between the deflector and the septum, if β_s and β_d are the values of the horizontal β-function at the septum and the deflector locations, then the angular kick is:

$$\theta = \frac{x}{\sqrt{\beta_s \beta_d}\sin\mu_x} \tag{8}$$

where x is the distance between the center of the injected beam and the center of the machine aperture at the location of the septum. Given the geometry of the vacuum chamber in this region, and taking into account the radius of the chamber (around 47 mm) and the septum thickness (around 10 mm), the distance x must be larger than 57 mm. Using equation (8), the required deflection angle is of the order of 4-5 mrad.

The maximum angular kick is needed for the injected beam, so that the center of the injected bunch is on the crest of the cosine deflecting field in the RF deflector. For a frequency multiplication factor of five, the centers of the four circulating bunches are located on the curve of the deflecting field with phases of $\frac{2\pi}{5}$, $\frac{4\pi}{5}$, $\frac{6\pi}{5}$, $\frac{8\pi}{5}$ from the crest. Shown in Figure 20 is the variation of the kick with the location of the bunches on the cosine curve.

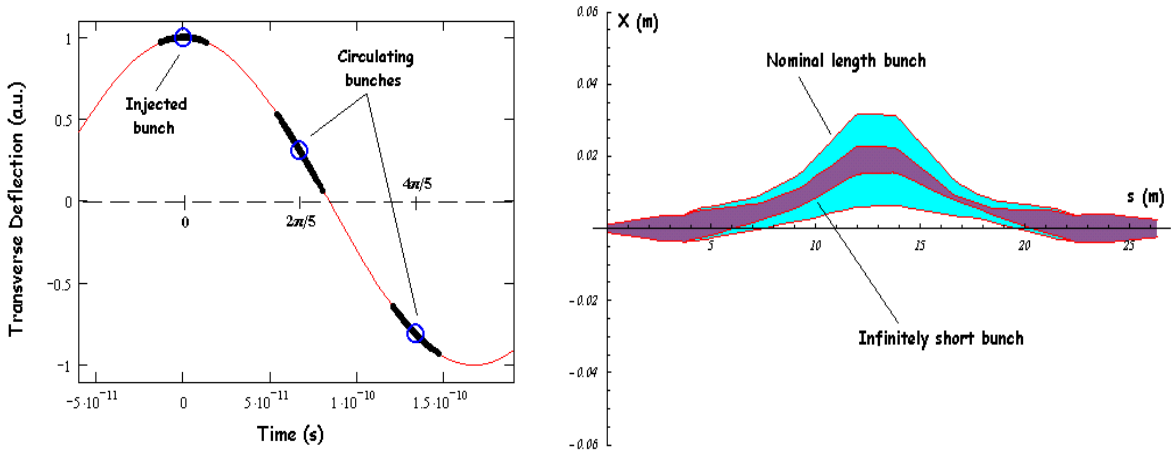

Figure 20: Left: Kick amplitudes for injected and circulating bunches for a combination factor of five. The next two circulating bunches are symmetrically located on the curve with respect to the minimum of the cosine. The extension corresponds to $\pm 2\sigma$ of a gaussian distribution with a length of 10 ps FWHM. Right: Beam envelopes in the cases of an infinitely short bunch and of a bunch with 10 ps FWHM. Both bunches have a rms normalized emittance of 40 π mm.mrad and are located at $2\pi/5$ on the RF curve.

As a consequence of the phase extension, the head and the tail of the circulating bunches experience different deflection angles. This enlarges the transverse size of the circulating beam in the region between the two RF deflectors. This effect represents the dominant contribution to the beam size at the level of the septum. The main constraints on the size of the beam are the limit of the vacuum chamber and the thickness of the septum in the chamber. In order to limit the phase extension, short bunches are essential, and simulations have shown that the maximum acceptable bunch length is around 15 ps FWHM for a combination factor of five.

The simplest injection process makes use of the RF deflectors only. However, it is also possible to use a combination of bumpers and RF deflectors. Indeed, to provide a significant reduction of the angular deflection needed from the RF deflectors, bumpers are also located close to the deflectors and can be used to add a static closed bump to the time-dependent bump of the deflectors.

Figure 21 shows the envelopes of gaussian bunches of length 10 ps FWHM (truncated longitudinally at $\pm 2\sigma$, with a 2σ extension in the transverse plane) in the injection region in the case of RF deflectors only. The deflection angle on the crest is the reference value 4.5 mrad. In this case, the circulating beam is deflected to the opposite side of the septum. On the other hand, Figure 22 illustrates the situation when the bumpers and the deflectors are used together. The deflection angle for the deflectors is 2.5 mrad on crest, and the angle in the bumpers is 2 mrad. In this case, the beam envelopes are shifted closer to the septum. Both methods seem experimentally feasible and provide some flexibility in operation.

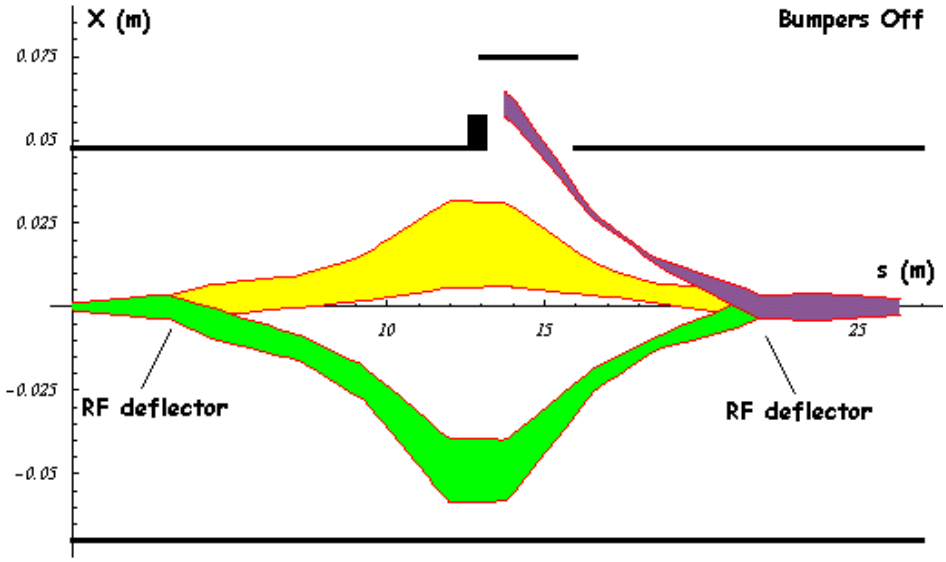

Figure 21: Beam envelopes of the injected and circulating beams (RF deflectors only) for a bunch length of 10 ps FWHM, longitudinally truncated at $\pm 2\sigma$. From top to bottom: injected bunch, circulating bunch with a phase of $\frac{2\pi}{5}$, and circulating bunch with a phase of $\frac{4\pi}{5}$. The straight lines are the limits of the vacuum chamber and the rectangle stands for the injection septum.

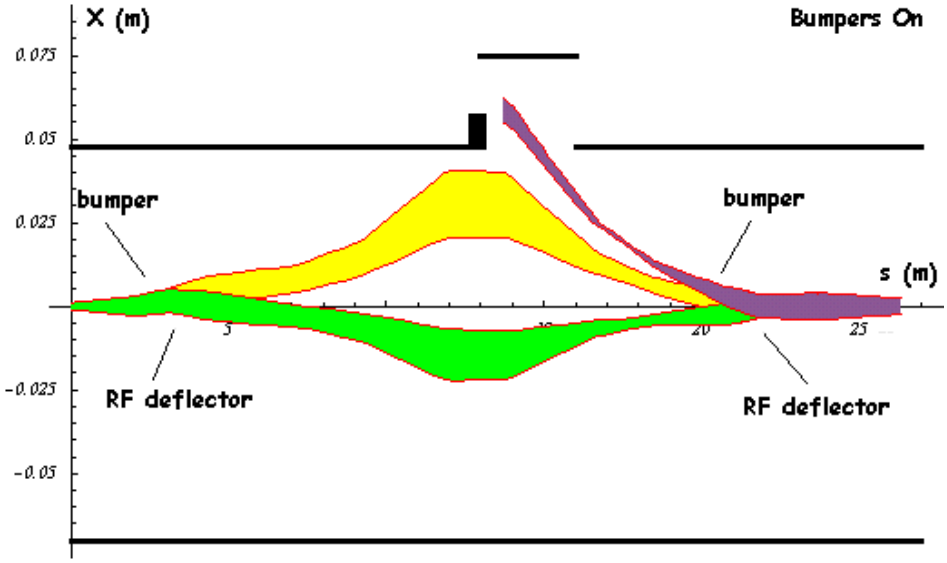

Figure 22: Beam envelopes of the injected and circulating beams (RF deflectors and bumpers) for a bunch length of 10 ps FWHM, longitudinally truncated at $\pm 2\sigma$. From top to bottom: injected bunch, circulating bunch with a phase of $\frac{2\pi}{5}$, and circulating bunch with a phase of $\frac{4\pi}{5}$. The straight lines are the limits of the vacuum chamber and the rectangle stands for the injection septum.

8 Complete tracking in the transfer line and in EPA

In order to check that the optics satisfies the requirements, a complete tracking through the modified transfer line and the isochronous ring has been carried out. Such a tracking allows to take into account the higher order effects in chromaticity and isochronicity in a global way. For this purpose, new tracking routines have been written on the basis of the MAD program, so as to generate realistic distributions of particles.

Longitudinally, the particles are distributed in time following a gaussian law and the momentum p is calculated for each particle using the formula:

$$p(t) = \cos(2\pi\nu t + \phi) \tag{9}$$

where ν is the RF frequency and ϕ is the RF phase. In this way, it is possible to describe the phase extension of the bunches on the RF curve, which is the main contribution to the energy spread within the bunches. In the transverse plane, the normalized phase space is considered and a unitary bi-gaussian distribution is generated. Knowing the emittance and the Twiss parameters, the transformation from the normalized phase space to the real phase space used for tracking is done through the inverse Floquet transformation defined as:

$$\begin{pmatrix} q \\ q' \end{pmatrix} = \begin{pmatrix} \frac{1}{\sqrt{\beta}} & 0 \\ -\frac{\alpha}{\sqrt{\beta}} & -\sqrt{\beta} \end{pmatrix} \begin{pmatrix} x \\ x' \end{pmatrix} \tag{10}$$

where (x, x') and (q, q') are respectively the variables in the real and normalized phase space, α and β being the Twiss parameters at the starting point.

The results of the tracking in the transfer line and the new EPA ring are presented in Figure 23. A tracking has also been performed through the matching section at the end of the linac, where no important aberration effects have been found. In the future, we intend to extend the analysis by starting the tracking at the beginning of the linac, after the front-end. For all simulations, the bunch length is set to 10 ps FWHM (or 1.28 mm rms), the normalized rms emittance is 40 π mm.mrad and the energy at the end of the linac is 350 MeV.

The left-hand side of the figure shows the tracking in the transfer line. The initial phase space is derived from the values of the Twiss parameters at the end of the linac (point zero), assuming a perfect matching between the linac and the transfer line. The final distributions result from one passage through the line. The right-hand side of the figure shows the tracking in the isochronous EPA ring. The initial distributions are the result from the tracking in the transfer line taken at the injection point, and the final distributions are given at the same point, after five turns in the ring. The difference between the initial and final transverse distributions indicate a small mismatch at the entrance in the ring. However, the discrepancy remains small. On the other hand, the longitudinal tracking shows no bunch lengthening. Less than 1% of the particles are lost after the tracking over five turns, mainly in the tails of the distributions. The tracking has been extended to 100 turns in the ring: the losses are kept at a low level (around 1.5%) and occur only in the first turns, which confirms the stability of the solution.

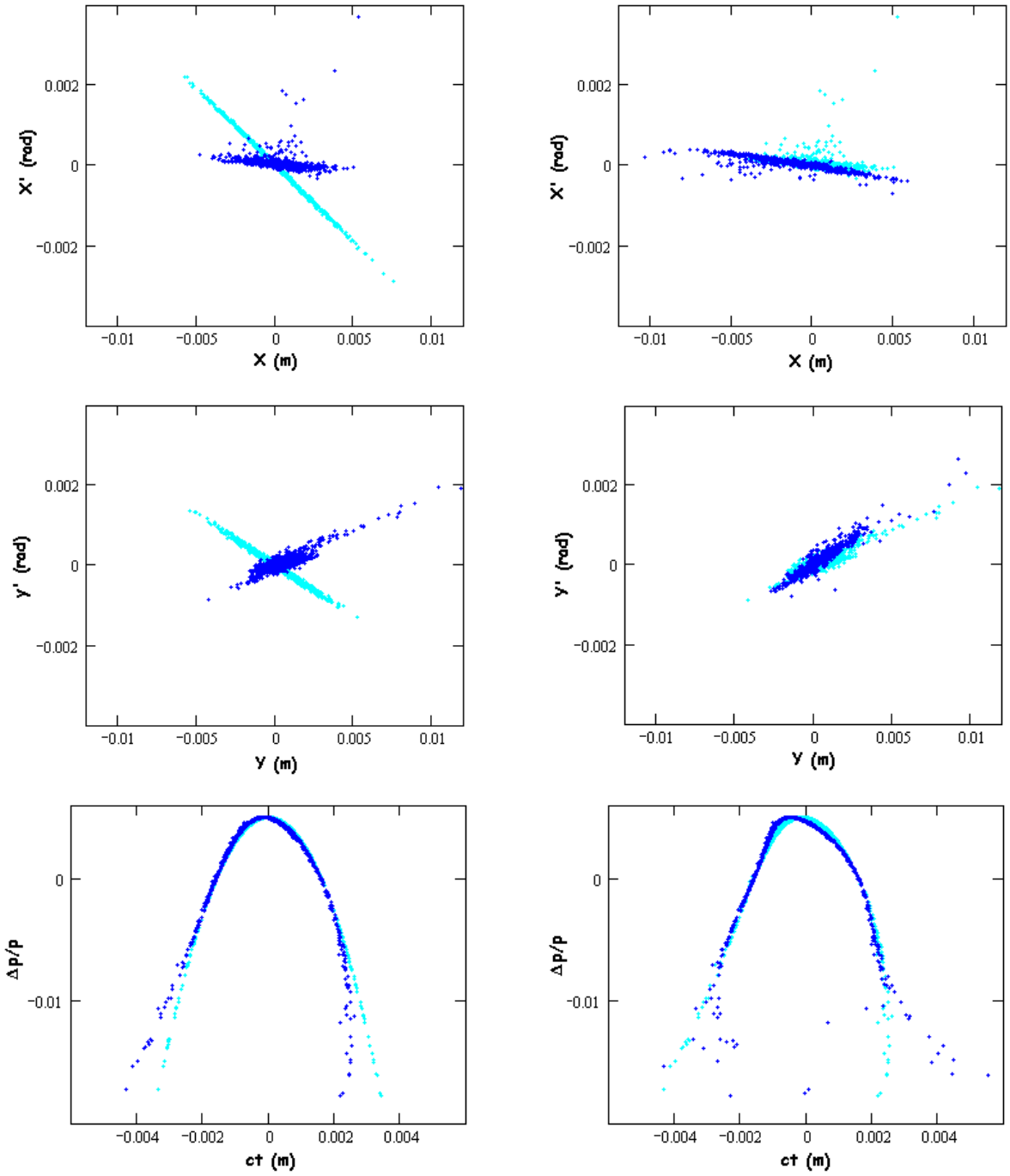

Figure 23: Complete transverse and longitudinal tracking in the transfer line (left-hand side), and in the isochronous ring after five turns (right-hand side). Light grey points are the initial distributions and dark grey points are the final distributions. The transverse horizontal phase space (top row), the transverse vertical phase space (middle row), and in the longitudinal phase space (bottom row) are shown. In each case, the tracking is done with 1000 particles.

9 Beam steering

Like for most the other elements of the CTF3 preliminary phase, Beam Position Monitors (UMAs) and correction magnets are re-used from the existing LPI complex. UMAs are installed in the front-end, the linac, the transfer lines and EPA. Small trim dipoles are distributed in the present installation, and a number of quadrupole magnets have separate windings that serve as correction dipoles. Their locations had to be verified with the modified optics for CTF3. This analysis was done for the linac with the optics described in section 4. Figure 24 shows the phase advance along the linac together with the monitor and corrector locations for both the horizontal and the vertical planes. It can be seen that the phase differences between the monitors are sufficiently small to sample the trajectory well. The distribution of the correction dipoles is also suitable for trajectory correction.

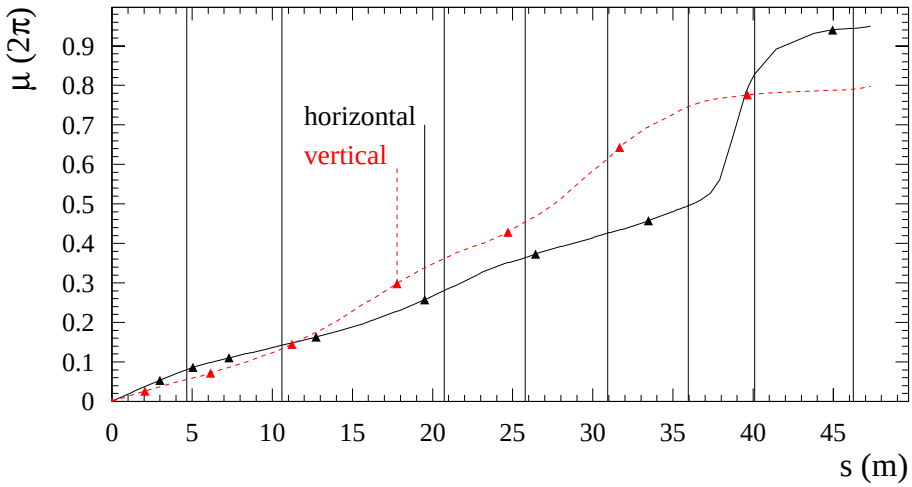

Figure 24: Phase advance along the linac starting at ACS28. The positions of the UMAs are indicated with vertical lines, and the positions of the trims are shown with triangles. The solid line corresponds to the horizontal direction, while the dashed line corresponds to the vertical direction.

Due to space restrictions, there is only one UMA installed in the transfer line but the additional diagnostics (see section 5.3) will enable a proper adjustment of the beam during commissioning.

The 19 existing UMAs in the EPA ring should be sufficient to ensure a good injection optimization and trajectory correction (the tunes are $Q_x \simeq 4.73$ and $Q_y \simeq 3.77$). The present ring has only two correction dipoles per transverse direction, but the installation of additional correctors is planned to ease the operation and to avoid the displacement of quadrupoles for trajectory correction.

It is envisaged to implement automated beam steering (ABS) for the linac, the injection line and the ring. This will be done in the framework of the general PS ABS project [30] with a description of the machine in the accelerator database [31]. The Electronic Data Management System (EDMS) is also a tool which is foreseen to be used in CTF3 [32].

10 Conclusions

In this note, we have given a description of the first stage of the CTF3 project (so called CTF3 preliminary phase) and we have presented the results of the corresponding beam dynamics studies. The main goal of the preliminary phase is to test the new scheme of electron pulse compression and bunch frequency multiplication, which is at the heart of the CLIC RF power source concept, at low bunch charge and with short pulses. It will provide a proof of principle of the scheme and it will be useful in order to gain experience and to test component prototypes, in view of the following stages of the project. The test will be performed in the area of the LPI complex, making use of existing components. While only a limited amount of new hardware will be used, several modifications to the existing installation are needed. They will be made during a dedicated shut-down period starting in April 2001. It is planned to begin the commissioning of the modified installation before the end of 2001, and to complete the bunch combination test by the end of 2002.

A number of beam dynamics studies were performed in order to assess the feasibility of the test and to identify the needed hardware changes. Both analytical and numerical calculations have been used, taking also into account the results of a series of beam measurements made on the existing installation [16, 17]. This analysis is now completed, and its results have been presented in this note. In particular, we have described in detail the new configuration and the corresponding optics for the front-end, the linac, the transfer line, and the ring.

The linac will be shortened and a new gun will be fitted into it. The beam parameters have been defined and the gun specifications have been identified. The existing bunching system and matching section to the linac will be used, and they should provide the desired performances in terms of bunch length ($\leq$ 10 ps FWHM) and charge ($q = 0.1$ nC). A new linac optics has been found, which requires only minimal hardware changes. A matching section between the linac and the transfer line to the ring has been designed. This new section provides a large flexibility, which is valuable for the typical mode of operation of a test facility. The design of the transfer line has been modified (without changing the positions and angles of the main bending dipoles) in order to be made isochronous and achromatic, and it has been transversally matched to the new ring optics. The ring layout will be slightly modified in order to obtain an optics which is isochronous and has a zero dispersion in the injection region, allowing for small beam sizes and good matching conditions at the injection. Chromatic corrections and second order isochronicity effects remaining at the desired level are achievable by using three sextupole families. The horizontal and vertical dynamic apertures are around 15σ for about 1000 turns, over the expected beam momentum spread ($\leq \pm$ 1%), which is comparable with the present performance. The variation of the total bunch length during the combination process (five turns) is negligible over this momentum range. This has been verified by tracking using the MAD code (including the transfer line). For this purpose, a complete six-dimension phase-space representation of the beam has been used, with realistic transverse and longitudinal distributions. The beam transverse stability has been checked as well. The new injection scheme with transverse RF deflectors was also studied. A couple of existing deflectors can provide the requested injection angle of

about 4.5 mrad and they will be used for injection. The beam envelopes in the injection region have been evaluted. A five-turn combination process is possible with low beam losses for bunches shorter than 15 ps FWHM, while for smaller combination factors the beam requirements on bunch length are relaxed.

The beam instrumentation in the whole complex has been reviewed and modified where necessary. In particular, the new matching section will be equiped with a spectrometer line and beam profile monitors. The installation will allow to perform time-resolved measurement with high resolution by using a streak camera and it will be used to fully characterize the beam at the end of the linac. A first check has also been made in order to check that the beam position monitors and the correction dipoles ensure a sufficent trajectory correction.

Appendix

The acronyms used in this note are summarized here:

- ACS = ACcelerating Structure
- CLIC = Compact LInear Collider
- CLIO = Collaboration pour un Laser à électrons libres dans l'Infrarouge à Orsay
- CTF3 = CLIC Test Facility 3
- EPA = Electron Positron Accumulator
- ECM = Electrode Capacitive Monitor (current monitor)
- HIE = (Hippodrome) Injection line for Electrons
- HIP = (Hippodrome) Injection line for Positrons
- INFN = Istituto Nazionale di Fisica Nucleare
- LAL = Laboratoire de l'Accélérateur Linéaire (Orsay)
- LEP = Large Electron Positron collider
- LIL = LEP Injector Linac
- LIPS = LIL Power Saver (RF pulse compression system)
- LPI = LEP Pre-Injector = LIL + EPA
- MDK = Modulator Klystron
- MSH = Monitor SEMgrid Horizontal (secondary emission monitor)
- MTV = Monitor TV
- PS = Proton Synchrotron accelerator
- SLH/SLV = SLit Horizontal/Vertical
- TCM = Transition-Cherenkov Monitor (profile monitor)
- UMA = pick-Up MAgnetic (beam position monitor)
- WBS = Wire Beam Scanner (profile monitor)
- WCM = Wall Current Monitor

References

[1] H.H. Braun, R. Corsini, T.E. D'Amico, J.P. Delahaye, G. Guignard, C.D. Johnson, A. Millich, P. Pearce, L. Rinolfi, A.J. Riche, R.D. Ruth, D. Schulte, L. Thorndal, M. Valentini, I. Wilson, W. Wünsch, "The CLIC RF power source: a novel scheme of two beam acceleration for electron-positron linear colliders", CERN-99-06 (1999).

[2] CLIC Study Team, "Proposals for Future CLIC Studies and a New CLIC Test Facility (CTF3)", CERN/PS 99-047 (LP) and CLIC Note 402 (1999).

[3] H. Braun, L. Rinolfi, "Technical description for the CLIO gun", CTF3 Note 2000-07.

[4] A. Pisent, L. Rinolfi, "A new bunching system for the LEP Injector Linac", CERN/PS/90-58 (LP).

[5] R. Corsini, J.P. Potier, L. Rinolfi, T. Risselada, "Isochronous Optics and Related Measurements in EPA", Proceedings of the 7th European Particle Accelerators Conference, Wien, June 2000.

[6] R. Corsini, B. Dupuy, A. Ferrari, L. Rinolfi, T. Risselada, P. Royer, F. Tecker, "LIL bunch length, LIL lattice parameters, LIL energy, LIL temperature versus RF frequency, EPA circumference and EPA isochronicity measurements", CTF3 note 2001-18 (MD), to be published.

[7] M.A. Tordeux, "Etude des longueurs de paquets du LIL à 4 MeV", PS/LP Note 93-14 (MD).

[8] W. Hermannsfeldt, "EGUN an electron optics and gun design", SLAC Report 331, October 1988.

[9] B. Mouton, "Proceedings of the fourth CTF3 collaboration meeting", CLIC Note 433, page 79, May 2000.

[10] "Etude, suivi de fabrication, tests au LAL, participation aux essais et mise en service au CERN d'un canon thermo-ionique type CLIO", Convention entre CERN et IN2P3, 26 May 2000.

[11] R. Chaput, "Electron gun for the FEL CLIO", Proceedings of 2nd EPAC Conference, Nice, 1990.

[12] J.C. Bourdon, R. Belbeoch, M. Bernard, P. Brunet, B. Leblond, M. Omeich, E. Plouviez, J. Rodier, "Commissioning the CLIO injection system", Nucl. Instr. Meth. in Physics Research A304 (1991) 322-328.

[13] A. Benscessan, D.T. Tran, D. Tronc, "High power standing wave triperiodic structure for positron acceleration", Nucl. Instr. Meth. 118 (1974) 349-355.

[14] J-C. Godot, L. Rinolfi, A. Pisent and H. Braun, "A new front-end for the LEP Injector Linac", CERN/PS/91-19 (LP), Proceedings of the 1991 Particle Accelerator Conference, 6-9 May 1991, San Francisco, California, USA.

[15] B. Mouton, "The PARMELA program, version 4.3", LAL/SERA 93-455.

[16] R. Corsini, A. Ferrari, L. Rinolfi, T. Risselada, P. Royer, F. Tecker, "LIL bunch length and lattice parameters measurements in March 2000", CTF3 Tech. Note 2000-09 (MD-LPI), PS/LP Note 2000-01 (MD).

[17] R. Corsini, A. Ferrari, L. Rinolfi, T. Risselada, P. Royer, F. Tecker, "New measurements of the LIL bunch length and lattice parameters", CTF3 Tech. Note 2000-13 (MD-LPI), PS/LP Note 2000-02 (MD).

[18] K.L. Brown, D.C. Carey, C. Iselin and F. Rothacker, "TRANSPORT, a computer program for designing charged particle beam transport systems", CERN 80-04.

[19] S. Battisti, M. Le Gras, J.M. Roux, B. Szeless, D.J. Williams, "Magnetic beam position monitors for the LEP Pre-Injector", CERN/PS 87-37-BR, IEEE, Particle Accelerators Conference, Washington D.C., March 1987.

[20] S. Battisti, "Measurement of the short bunch length in the CLIC test facility", CERN/PS 93-40, CLIC Note 211.

[21] J.C. Thomi, "La mesure de profils longitudinaux de faisceaux d'électrons", PS/BD/Note 93-03.

[22] H. Grote and F.C. Iselin, "The MAD Program", CERN/SL 90-13 (AP), 1993.

[23] L. Groening, private communication.

[24] T. Risselada, "An isochronous optics for EPA", PS/LP Note 99-02 (tech).

[25] R. Corsini, J.P Potier, L. Rinolfi, T. Risselada, J.C. Thomi, "First micro-bunch measurements in EPA as isochronous ring at 500 MeV", PS/LP Note 99-03 (MD).

[26] R. Belbeoch, "Utilisation d'une section accélératrice pour la mesure du profil longitudinal des micro-paquets à la sortie du groupeur de la station d'essais du LAL", SERA Note 89-09.

[27] Ph. Bernard, H. Langeler and V. Vaghin "On the design of disk-loaded waveguides for RF separators", CERN 68-30 (1968).

[28] S. Gallo, "Proceedings of the first CLIC/CTF3 collaboration meeting held at CERN, 3-5 May 1999", CLIC Note 401, page 215.

[29] I. Syratchev, private communication.

[30] B. Autin, V. Ducas, A. Lombardi, M. Martini and E. Wildner, "Automated Beam Optics Correction for Emittance Preservation", CERN-PS-97-007-DI, 3rd International LHC Workshop: High-brightness Beams for Large Hadron Colliders, 13-18 Oct 1996, Montreux, Switzerland.

[31] B. Autin, F. Di Maio, M. Gourber-Pace, M. Lindroos and J. Schinzel, "Database for accelerator optics", CERN-PS-97-065, International Conference on Accelerator and Large Experimental Physics Control Systems, 3-5 Nov 1997, Beijing, China.

[32] L. Rinolfi, J. Schinzel, "CTF3 Project Information Management Proposal", CTF3 Note 2000-017 (EDMS).